Biological classification of memory clinic patients

Sophie E. Mastenbroek,[1,2,3] Lyduine E. Collij,[1,2,3] Toomas Erik Anijärv,[1] Jonathan Rittmo,[1,4] Alexandra L. Young,[5] Olof Strandberg,[1] Ruben Smith,[1,6] Nicola Spotorno,[1] Sebastian Palmqvist,[1,6] Niklas Mattsson-Carlgren,[1,6,7] Shorena Janelidze,[1] Piero Parchi,[8,9] Jacob W. Vogel,[1,4] Frederik Barkhof,[2,3,10] Rik Ossenkoppele[1,11,12] and Oskar Hansson[1]

Abstract

Neurodegenerative diseases have traditionally been defined *in vivo* based on clinical symptoms. However, the development of biomarkers has enabled a shift toward *in vivo* biological definitions. There is now a need to characterize memory clinic populations using multi-dimensional biomarker information. Here, we employed a data-driven approach to develop a biological framework for categorizing individuals in a heterogenous memory clinic cohort based on the presence, extent, and sequence of several common pathologies.

We studied 1,677 individuals, including subjective cognitive decline (SCD, *n*=255), mild cognitive impairment (MCI, *n*=400), all cause dementia (*n*=393), and cognitively normal controls (*n*=625) from the BioFINDER-2 cohort (median age [IQR]=72.0 [16.2] years; 50.3% female). The Subtype and Stage Inference (SuStaIn) model was applied to biomarkers of amyloid-β (Aβ) (cerebrospinal fluid [CSF] $A\beta_{42}/A\beta_{40}$), tau (temporal meta-ROI positron emission tomography [PET]), neuronal α-synuclein (CSF seed amplification assay [SAA]), vascular pathology (MRI-based white matter hyperintensities [WMHs]), and regional atrophy (MRI-based cortical thickness) to identify biomarker-based clusters across the entire dataset. We then applied this framework to cognitively symptomatic individuals (*n*=788) to compare clinical symptoms, disease progression rate, and brain changes (atrophy and functional connectivity) across profiles.

We identified five biomarker clusters reflecting established clinico-pathological entities, closely corresponding to (i) Alzheimer's disease (AD, *n*=317 [40.2%]); (ii) α-Synuclein disease (αSyn, *n*=123 [15.6%]), (iii) Vascular disease (*n*=67 [8.5%]); (iv) Mixed AD and Vascular diseases (Mixed, *n*=207 [26.3%]); and (v) a heterogenous group of individuals characterized by atrophy without any of the major brain pathologies, here termed Non-Vascular-Alzheimer-Synuclein (NOVAS, *n*=74 [9.4%]). The AD profile was characterized by global cognitive impairment and cortical atrophy in AD-associated regions. The αSyn profile was associated with visuospatial and executive dysfunction, motor impairment, hallucinations, and functional connectivity disruptions throughout the brain, despite less overall atrophy compared to all others. The Vascular profile showed language and motor impairments and both the Vascular and Mixed profiles demonstrated atrophy in cingulate and subcortical regions, alongside reduced periventricular white matter integrity. The NOVAS profile was older, demonstrated pronounced hippocampal and amygdala atrophy, and baseline memory deficits, possibly reflecting neurodegenerative diseases for which currently no robust biomarkers are available, such as primary tauopathies and TDP-43 proteinopathies (e.g. LATE). In longitudinal analyses, the AD profile showed the fastest global cognitive decline, while αSyn demonstrated an accelerated decline in language, executive, and visuospatial functioning.

To conclude, classifying individuals using a multimodal biomarker approach can provide valuable diagnostic and prognostic insights, with potential implications for clinical trials.

Author affiliations:

1 Clinical Memory Research Unit, Department of Clinical Sciences Malmö, Faculty of Medicine, Lund University, 222 42 Lund, Sweden

2 Department of Radiology and Nuclear Medicine, Vrije Universiteit Amsterdam, Amsterdam University Medical Center, location VUmc, 1081 HV Amsterdam, The Netherlands

3 Amsterdam Neuroscience, Brain imaging, 1081 HV Amsterdam, The Netherlands

4 Department of Clinical Sciences, SciLifeLab, Lund University, 222 42 Lund, Sweden

5 UCL Hawkes Institute, Department of Computer Science, University College London, WC1V 6LJ London, UK

6 Memory Clinic, Skåne University Hospital, 205 02 Malmö, Sweden

7 Wallenberg Center for Molecular Medicine, Lund University, 223 62 Lund, Sweden

8 IRCCS, Istituto delle Scienze Neurologiche di Bologna (ISNB), 40139 Bologna, Italy

9 Department of Biomedical and Neuromotor Sciences, University of Bologna, 40127 Bologna, Italy

10 Queen Square Institute of Neurology and Centre for Medical Image Computing, University College London, WC1N 3BG London, UK

11 Alzheimer Center Amsterdam, Neurology, Vrije Universiteit Amsterdam, Amsterdam UMC location VUmc, 1081 HV Amsterdam, The Netherlands

12 Amsterdam Neuroscience, Neurodegeneration, 1081 HV Amsterdam, The Netherlands

Correspondence to: Sophie E. Mastenbroek

Clinical Memory Research Unit, Department of Clinical Sciences Malmö, Lund University

Klinikgatan 28, room C1103b, SE-222 42 Lund, Sweden

E-mail: sophie.mastenbroek@med.lu.se

Correspondence may also be addressed to: Oskar Hansson

Clinical Memory Research Unit, Department of Clinical Sciences Malmö

BMC C11, Lund University, Box 117, SE-22100 Lund, Sweden

E-mail: oskar.hansson@med.lu.se

Running title: Biological classification of patients

Keywords: amyloid-β; tau, α-synuclein; vascular; biological framework; data-driven

Introduction

Neurodegenerative diseases have traditionally been defined clinically as syndromes that are based on clusters of cognitive and neurological symptoms, with the most common clinical disorders being Alzheimer's disease (AD)[1], followed by vascular dementia (VaD)[2], and Lewy body disease (LBD)[3,4]. The availability of biomarkers enables a paradigm shift towards an *in vivo* biological definition of neurodegenerative diseases[5,6]. For some time, fluid and imaging markers of misfolded amyloid-β (Aβ) and tau have been clinically available[5,7-9], together with magnetic resonance imaging (MRI) for the detection of atrophy and cerebral small vessel disease (cSVD) markers, such as white matter hyperintensities (WMHs), infarcts, lacunes, and microbleeds[10,11]. More recently, in vitro seed amplification assays (SAAs) have been developed to detect misfolded alpha-synuclein (α-syn) in the cerebrospinal fluid (CSF)[12], achieving high diagnostic accuracy in detecting Lewy body (LB) pathology[13-16]. While biological definitions have been proposed for neurodegenerative diseases[5,17,18], efforts to comprehensively characterize memory clinic populations using extensive multi-dimensional biomarker information, including the CSF SAA, are limited.

Many neurodegenerative pathologies commonly co-occur within the same individuals[19-24], with up to 80% of elderly individuals with a neurodegenerative disease having more than one pathology in the brain[25]. While one pathology is usually the primary driver of symptoms, the presence of multiple pathologies negatively affects clinical outcomes[26-29]. This highlights the importance of assessing the presence of all relevant biomarkers collectively, particularly in the context of individual prognosis and clinical trial selection. However, our understanding of the evolution of comorbidities in vivo is limited, including the order in which multiple pathologies emerge, and how this progression influences clinical outcomes.

In this study, we applied a machine learning method to baseline biomarker data, in order to identify clusters of individuals with similar biomarker profiles, while simultaneously estimating the temporal evolution of pathologies[30-32]. Next, we characterized these biomarker profiles in patients with cognitive complaints to characterize the biomarker-based clusters regarding clinical symptoms, disease progression rate, and changes in brain structure and function.

Materials and methods

Study cohort

Participants were included from the prospective BioFINDER-2 cohort (NCT03174938, http://www.biofinder.se/), which spans the full spectrum of the AD continuum, ranging from neurologically and cognitively healthy controls, adults with subjective cognitive decline, mild cognitive impairment (MCI) to AD dementia, as well as patients with non-AD neurodegenerative diseases. All participants were recruited at Skåne University Hospital and the Hospital of Ängelholm, Sweden. Detailed inclusion and exclusion criteria have been previously described[33]. In brief, participants were considered cognitively unimpaired (CU) if they did not meet the criteria for mild cognitive impairment (MCI) or dementia as outlined by the DSM-5[34]. Participants were classified as MCI if they did not meet the criteria for dementia according to the DSM-5, and performed below 1.5 standard deviations from normative scores[35] in at least one cognitive domain, including verbal fluency, episodic memory, visuospatial ability, and attention/executive functioning[28]. Participants with dementia were classified according to the DSM-5 criteria for major neurocognitive disorders[34]. A clinical diagnosis of AD was based on the DSM-5 criteria for mild or major neurocognitive disorders due to AD and amyloid positivity in CSF in agreement with the International Work Group (IWG) criteria of AD (see methods for establishing biomarker positivity)[36]. A clinical diagnosis of DLB was based on the McKeith criteria for probable DLB[37,38] and PD was diagnosed using the Gelb criteria[39]. Dopamine Transport (DAT) scans were used as a supportive biomarker when available. Participants meeting criteria for both AD and DLB or PD were classified as having DLB or PD. Vascular dementia was diagnosed according to the DSM-5 criteria for mild or major vascular neurocognitive disorder[34] and required significant vascular changes on MRI (i.e., Fazekas score ≥2 or strategical infarcts). Additional diagnoses (frontotemporal dementia, progressive supranuclear palsy, multiple system atrophy, corticobasal syndrome, or semantic variant primary progressive aphasia) were assigned as previously described[40]. The study was approved by the Regional Ethics Committee in Lund, Sweden, and all participants provided written informed consent.

Detailed sample selection is shown in **Fig. 1.** Briefly, to identify biomarker-based profiles, we selected 1,677 participants from the total BioFINDER-2 cohort (n=2,581) with baseline data on

CSF SAA-derived α-syn status, CSF $A\beta_{42}/A\beta_{40}$, tau-PET, and MRI measures. Comparisons between included and excluded participants are demonstrated in **Supplementary Table 1**. 788 individuals (cognitively symptomatic, SuStaIn stage>0, and subtype assignment probability >50%) were subsequently included in the statistical analysis (see Statistical Analysis section). A subset of those also had baseline amyloid-PET (*n*=415), functional MRI (fMRI) (*n*=553), diffusion tensor imaging (DTI) (*n*=711), and clinical assessments (*n* varying by assessment, see **Supplementary Table 2** for details). In addition, a subset of participants underwent longitudinal clinical assessments (*n* and follow-up time varying by assessment, see **Supplementary Table 2** for details).

Cerebrospinal fluid markers

Amyloid-positivity was determined using the CSF $A\beta_{42}/A\beta_{40}$ ratio, with either the Elecsys immunoassay (Roche Diagnostics[41], cutoff=0.080[40]) or, if that was not possible, the Lumipulse G immunoassay (cutoff=0.072)[42]. CSF Neurofilament Light (NfL) levels were measured with the NULISA panel. LB status was determined through CSF α-syn SAA testing, as described previously[28,29].

Aβ- and tau-PET acquisition and processing

PET images were acquired using digital GE Discovery MI scanners. Tau-PET imaging was performed 70-90 minutes post-injection of ~370 MBq [^{18}F]RO948, and Aβ-PET imaging was acquired 90–110 minutes post-injection of ~185 MBq [^{18}F]Flutemetamol. Images were processed using an in-house pipeline as previously described[43]. Briefly, PET images were attenuation-corrected, motion-corrected, averaged, and registered to the closest T1-weighted MRI scan. Standardized uptake value ratio (SUVR) images were created using cortical parcellations (FreeSurfer v6.0), with the inferior cerebellar gray matter as the reference region for [^{18}F]RO94858 and the whole cerebellum for [^{18}F]Flutemetamol.

Tau-[^{18}F]RO948 positivity was evaluated in a volume-weighted composite region of interest (ROI) corresponding to Braak stages I-IV (average of bilateral entorhinal cortex, inferior/middle temporal, fusiform gyrus, parahippocampal cortex, and amygdala)[44], using a pre-determined cut-off of 1.36 SUVR[43]. Additionally, continuous [^{18}F]RO948 and [^{18}F]Flutemetamol SUVRs were extracted for the 68 bilateral regions of the Desikan-Killiany (DK) atlas[45].

Magnetic resonance imaging acquisition and processing

MRI scanning was performed using a 3T MAGNETOM Prisma scanner (Siemens Healthineers). Cortical thickness and deep gray matter volume estimates were extracted from structural T1-weighted MRI images using FreeSurfer version 6.0 as previously described[46] and FSL-FIRST v5.0.0[47,48], respectively. All volumes were adjusted for intracranial volume (ICV) (i.e., volume/ICV). Surface area-weighted composite measures were computed for whole brain (average of bilateral cortical regions) and AD-signature (average of bilateral entorhinal, inferior/middle temporal, and fusiform gyrus) cortical thickness. Additionally, bilateral lateral ventricular volume, normalized for ICV, was estimated as a measure of central atrophy. Cutoffs for dichotomous global (<2.18), AD-signature (<2.38), and central atrophy (>0.04) abnormalities were calculated as 2 standard deviations below the mean of an Aβ-negative CU reference population (n=691).

Resting-state fMRI data were acquired with a 3D echo-planar imaging (EPI) sequence with an in-plane resolution of 3×3 mm and slice thickness of 3.6 mm, echo time=30ms, and flip-angle=63°. Scan time was 7.85 minutes, with a multiband repetition time of 1020 ms. Preprocessing was performed using a modified CPAC pipeline[49] briefly described before[50], including slice-timing and motion correction, bandpass filtering (0.01–0.1 Hz), as well as regression of motion parameters[51], physiological noise[52], white matter, and CSF signals, linear and quadratic trends. High-motion frames were censored based on DVARS[53]. Native images were registered to MNI space, smoothed with a Gaussian filter (6 mm full-width at half maximum), and parcellated using the Schaefer 400 atlas[54]. Connectivity matrices were generated as pairwise Pearson correlations between parcels, with negative correlations set to zero. Nodal connectivity strength was calculated as the mean of each column in the matrix, yielding one value per parcel per subject[55]. Global

connectivity was quantified as the mean of all values between all region pairs. Images with a mean frame displacement (FD)≤0.03 mm and maximum FD≤3.0 mm were included (*n*=553).

Multi-shell diffusion weighted images (DWI) were acquired using a single-shot echo-planar imaging sequence (TR/TE=3500/73ms, 104 volumes, b-values span 0, 100, 1000, 2500 s/mm², with diffusion directions distributed across 2, 6, 32, and 64 orientations). DWI data were processed using an in-house pipeline that combines tools from MRtrx3[56] and FSL[48]. To assess microstructural integrity, diffusion tensor imaging (DTI) was applied to the DWI series including data with b-values up to 1000 s/mm² using the weighted least-squares method[57]. Fractional anisotropy (FA) and mean diffusivity (MD) maps were then derived from the tensor model[58].

Whole-brain WMH volumes were measured using the FreeSurfer-based Lesion Segmentation Tool[59] and normalized for ICV (volume/ICV). A cutoff of 0.005 mm^3, defined as the third tertile of WMH volumes, was applied to derive a dichotomous measure of small vessel disease (cSVD)[60]. Regional WMH volumes were segmented from a 3D T2-Fluid attenuated inversion recovery (FLAIR) sequence using Bayesian Model Selection (BaMOS)[61]. We estimated the average ICV-normalized WMH volumes in the frontal, parietal, temporal, and occipital lobes.

Cardiovascular risk score

For 543 participants, we computed the office-based Framingham Heart Study Cardiovascular Disease (FHS-CVD) risk score at baseline, which estimates the probability of cardiovascular events occurring within 10 years of risk assessment[62]. The FHS-CVD risk score is a sex-specific multi-variable weighted risk score based on self-reported age, body mass index (BMI), systolic blood pressure (SBP), antihypertensive treatment, diabetes status, and current cigarette smoking.

Clinical outcomes

Global cognitive functioning was assessed with the Mini-Mental State Examination (MMSE). Specific cognitive domains were tested, including memory (z-scored [reference=691 CU individuals] memory composite including ADAS immediate and delayed recall), language

(categorical fluency), executive functioning (symbol digit modalities test [SDMT] and trail making test [TMT] B – TMT A), attention (TMT A), and visuospatial functioning (incomplete letter test from the Visual Object and Space Perception [VOSP] battery).

Smell function was assessed using the ODOFIN Burghart Sniffin' Sticks (MediSense)[63]. Motor function was measured using the total score from the motor section of the informant-based Cognitive Impairment Questionnaire (CIMP-QUEST)[64]. The presence of hallucinations was assessed using the Mild Behavioral Impairment Checklist (MBI-C)[65] and symptoms of depression and anxiety were assessed with the Hospital Anxiety and Depression Scale (HADS)[66].

Biomarker profiling using SuStaIn

Biomarker subtyping and staging were performed through disease progression modeling using the Ordinal SuStaIn implementation in PySuStaIn[31,32]. In the entire sample of cognitively normal controls and cognitively symptomatic individuals, SuStaIn was applied to cross-sectional biomarker data of Aβ (CSF $A\beta_{42}/A\beta_{40}$), tau (tau-PET Braak I-IV), neuronal α-syn (CSF α-syn SAA), vascular pathology (MRI-derived WMH volume), and atrophy (MRI-derived global and AD-signature cortical thickness, and lateral ventricular volume), to identify data-driven biomarker profiles based on the inferred temporal evolution of these biomarkers. To ensure consistency with the CSF SAA measure, which is inherently binarized, we chose to binarize all biomarkers using pre-established cutoffs as described above. However, to retain some degree of quantitative information where possible, we further stratified the biomarker-positive group into low and high burden subgroups by a median split for tau, vascular, and atrophy biomarkers. The Ordinal implementation of SuStaIn requires as input the probability that a biomarker is normal or abnormal regarding amyloid and neuronal α-syn biomarkers, and normal, abnormal with low burden, or abnormal with high burden regarding all other biomarkers[31]. Probabilities were computed by estimating a normal distribution with a standard deviation of 0.5 around each score and normalizing the sum of the probabilities[67,68] (**Supplementary Table 3**).

The number of clusters was determined using the cross-validation information criterion (CVIC) and log-likelihood, estimated via 10-fold cross-validation[30]. Each participant was assigned to a biomarker profile and stage, with the stage serving as a proxy for progression along the inferred

sequence of biomarker abnormality. In our study, 12 stages were modeled for each profile. Participants were assigned to stage 0 if it was most likely that all of their biomarkers were normal. In addition, SuStaIn assigns each individual a probability of belonging to each SuStaIn profile, based on how well their biomarker profile fits the progression pattern inferred by the model. These probabilities reflect the degree of certainty of the current SuStaIn profile assignment relative to the alternative SuStaIn profiles. For subsequent statistical analyses, only subjects with a SuStaIn stage>0 and a confident profile assignment (probability >50%) were included, in line with prior SuStaIn publications[30,69,70].

Statistical analysis

For statistical analyses, only subjects with a SuStaIn stage>0, a confident profile assignment (>50%), and a diagnosis of SCD, MCI, or dementia were included (n=788). Baseline characteristics of memory clinic patients (SCD, MCI, and dementia) with low certainty in profile assignment (n=85) are detailed in **Supplementary Table 4**. Biomarker profiles were compared to each other according to a one-vs-all approach, *i.e.*, determining unique characteristics of each profile compared to all others. First, baseline differences in demographics, cardiovascular risk factors, and biomarker abnormalities were compared using Kruskal-Wallis and chi-squared tests, as appropriate. Next, a combined multinomial logistic regression model was used to determine the effect of clinical status, age, sex, years of education, *APOE* ε2 and ε4 status, diabetes, and hypertension on profile assignment. Biomarker profile differences in global and regional amyloid-PET, tau-PET, WMHs, CSF NfL, cortical thickness, subcortical volumes, and functional connectivity were assessed with linear models adjusted for age and sex, and fMRI models additionally included mean FD. Linear mixed models (LMMs) with an interaction between biomarker profile and time were performed to investigate baseline (main effect of biomarker profile) and longitudinal (baseline biomarker profile x time) differences in cognition. LMMs included random intercepts and random slopes and were adjusted for age, sex, and years of education. Voxel-wise statistical analysis of FA and MD was performed using Tract-Based Spatial Statistics (TBSS)[71], included in FSL[47]. TBSS create a white matter "skeleton" based on the individual FA maps before applying voxel-wise cross-subject statistical comparisons. Statistical

comparisons for each subtype (1-5) against all other subtypes combined were performed using non-parametric testing as implemented in FSL's 'randomise' with 5,000 permutations and threshold-free cluster enhancement for multiple comparison correction. This process was conducted with two distinct design matrices: one including age and sex as covariates, and the other with age, sex, and cognitive status at baseline. Both positive and negative contrasts were evaluated for each metrics, with statistical significance set at $p<0.05$.

Analyses were performed in R version 4.4.2[72]. Significance was set at two-sided $P<0.05$. All comparisons were false discovery rate-corrected for multiple comparisons based on the number of models within different subcategories of analyses (amyloid-PET, tau-PET, WMH volumes, atrophy, functional connectivity, TBSS, and cognition). As a supplementary analysis, all comparisons were additionally adjusted for cognitive status at baseline. A healthy aging reference group (cognitively unimpaired, no pathology, age>60 years, *n*=143) was included in figures only as a visual reference (**Fig. 1**).

Results

Characteristics of the SuStaIn modelling cohort

Baseline characteristics for the entire SuStaIn modeling cohort and stratified by cognitive status are provided in **Supplementary Table 5**. Among the 1,677 participants included in the SuStaIn modelling, 625 (37.3%) were CU, 255 (15.2%) had SCD, 400 (23.9%) had MCI, and 393 (23.5%) had dementia. The median age was 72.0 years (IQR=16.2), 50.3% were female, and the median FHS-CVD risk was 27.2 (IQR=29.5). 50.5% were *APOE* ε4 carriers, and 10.2% were ε2 carriers. Among those with cognitive impairment, 48.1% had a clinical diagnosis of AD, 5.5% had VaD, 6.0% had DLB, 4.3% had PD, 14.0% had another neurodegenerative disease diagnosis, and 22.1% (MCI=17.7%; dementia=4.4%) had an unclear diagnosis that was yet to be determined. Regarding biomarker status, abnormal CSF Aβ levels were the most common (46.0%), followed by WMH (32.7%), tau (22.4%), atrophy (AD signature [18.8%]; central [18.3%]; global [15.8%]), and neuronal α-syn (17.5%).

Five biomarker-based profiles with distinct temporal ordering

Based on model fit statistics from 10-fold cross-validation, five biomarker-based profiles best represented the data (**Supplementary Fig. 1**). Based on the overall clinico-pathological appearance of these data-driven profiles, they were termed: "AD", "α-Synuclein (αSyn)", "Vascular", "Mixed AD & Vascular" (Mixed), and "Non-Vascular-Alzheimer-Synuclein (NOVAS)" (**Fig. 2**).

The AD profile exhibited a typical AD disease progression, with early abnormalities in Aβ and tau pathology, followed by AD-signature atrophy and global atrophy. In the αSyn profile, neuronal α-Synuclein pathology emerged first, followed by Aβ pathology, WMHs, tau pathology, and finally atrophy. The Vascular profile was marked by early WMHs and atrophy, particularly central and global atrophy. Like the AD profile, the Mixed profile also followed an AD-like trajectory, but with the key distinction of an early vascular component, including WMHs and central atrophy. Finally, the NOVAS profile was characterized by early Aβ pathology and atrophy, with tau abnormalities appearing last. Notably, uncertainty regarding the temporal sequence of biomarker abnormalities increased in later SuStaIn stages.

Biomarker profiling and staging

Out of 1,677 participants, 556 (33.2%) were assigned a stage of 0. Information on the baseline characteristics of these individuals is provided in **Supplementary Table 6**. The median certainty of profile assignment was 75.5% (IQR=58.7%-98.1%), with the lowest certainty observed in the early and late stages (**Supplementary Fig. 2A**). Among those included in subsequent statistical analyses (subtype probability>0.5; cognitively symptomatic; *n*=788; **Fig. 1**), the majority were assigned to the AD profile (317 [40.2%]), followed by the Mixed profile (207 [26.3%]), αSyn (123 [15.6%]), the NOVAS profile (74 [9.4%]), and the Vascular profile (67 [8.5%]). Most participants were assigned to early biological stages (61.7%), indicating abnormalities in only one to three biomarkers (**Supplementary Fig. 2B**).

Biomarker profiles show distinct baseline characteristics

Detailed baseline characteristics and comparisons are presented in **Table 1**. Compared to the other profiles, the AD profile had a significantly higher percentage of *APOE* ε4 carriers (χ^2=60.7, p<.001). Individuals assigned to the αSyn and Vascular profiles were significantly more likely to be male ($\chi^2_{\alpha Syn}$=13.3, $p_{\alpha Syn}$<.001; $\chi^2_{Vascular}$=11.9, $p_{Vascular}$=.001). The Vascular profile exhibited significantly more vascular risk factors (χ^2=19.1, p<.001) and the Mixed profile had a significantly higher percentage of *APOE* ε2 carriers (χ^2=8.2, p=.004). Compared to the other profiles, individuals assigned to the NOVAS profile were significantly more likely to have dementia (χ^2=5.8, p=.016). They also had a significantly lower baseline global cognition, as indicated by the MMSE (χ^2=5.2, p=.022), and were, on average, older (χ^2=17.2, p<.001). Combining all variables into a multivariable logistic regression in general revealed similar profile differences (**Supplementary Table 7**).

The distribution of baseline clinical diagnoses across biomarker profiles is illustrated in **Fig. 3**. The AD biomarker profile consisted primarily of "clinical AD" (66.2%) and individuals with "SCD" (21.5%). The αSyn profile was dominated by "clinical LB disease" (20.3% DLB; 19.5% PD), alongside "clinical AD" (29.3%). The Vascular profile comprised mainly "clinical VaD" (17.9%), "undetermined" (26.9%), and "other" diagnoses (23.9%). A detailed description of the "other" group can be found in **Supplementary Table 8**. The Mixed biomarker profile similarly consisted for the majority of "clinical AD" (34.8%) and "SCD" (24.6%) but also contained "clinical VaD" (10.1%) and "undetermined" (16.9%) diagnoses. The NOVAS profile was characterized mainly by "other diagnosis" (31.1%), which predominantly included frontotemporal lobar degeneration (FTLD) spectrum disorders (n=19). Additionally, NOVAS included "undetermined" (25.7%) and "clinical AD" (21.6%) diagnoses, which, with one exception, were not atypical AD cases (see **Supplementary Table 9** for profile assignment of atypical AD cases). The distribution of biomarker profile assignment across clinical groups is illustrated in **Supplementary Fig. 3**.

Biomarker profiles are associated with distinct cognitive profiles at baseline

Regarding baseline cognitive performance, the AD biomarker profile demonstrated worse global cognition, as measured by the MMSE (β=-0.24, p_{FDR}<.001), but fewer depressive (HADS: β=-0.25, p_{FDR}=.004) and motor (CIMP: β=-0.51, p_{FDR}<.001) symptoms and hallucination (MBI-C5: β=-0.89, p_{FDR}=.039) compared to all other profiles (**Fig. 4**, **Supplementary Table 10**). The αSyn profile was associated with worse baseline performance in language (categorical fluency: β=-0.04, p_{FDR}=.024), executive functioning (TMT B-A: β=0.05, p_{FDR}<.001), and visuospatial functioning (VOSP: β=-0.46, p_{FDR}=.024). It also exhibited more severe depressive symptoms (HADS: β=0.19, p_{FDR}=.044), greater motor impairment (CIMP: β=0.34, p_{FDR}<.001), and a higher prevalence of hallucinations (MBI-C5: β=1.90, p_{FDR}<.001) compared to all other profiles. The Vascular biomarker profile exhibited poorer language performance (categorical fluency: β=-0.17, p_{FDR}=.024), more severe motor symptoms (CIMP: β=0.64, p_{FDR}<.001), and less severe visuospatial impairments (VOSP: β=0.04, p_{FDR}=.024) relative to all other profiles. The Mixed biomarker profile had better global cognition (MMSE: β=0.23, p p_{FDR}<.001) and executive functioning (TMTB-A: β=-0.10, p p_{FDR}=.040) than all others. Finally, the NOVAS group exhibited worse baseline memory performance (ADAS memory composite: β=0.15, p_{FDR}=.028) and worse attention (TMT A: β=0.01, p_{FDR}=.028) compared to the others. Results from models adjusted for cognitive baseline status were largely consistent (**Supplementary Table 11).**

Biomarker profile comparisons of regional Aβ, tau, and WMHs at baseline

Next, we conducted detailed spatial comparisons of the biomarker profiles on key baseline pathologies included in the SuStaIn model – Aβ- and tau-PET, and WMHs. Detailed global and regional comparisons can be found in **Supplementary Fig. 4**. Generally, the biomarker profiles followed expected patterns across biomarkers. Notably, individuals in the Mixed profile exhibited, compared to all others, lower baseline global Aβ- and temporal-parietal tau-PET uptake but greater

cross-sectional WMH volumes across all brain lobes. The NOVAS biomarker profile showed, on average, lower tau burden compared to the other profiles.

Biomarker profiles reveal differences in atrophy, functional connectivity, and white matter integrity

Atrophy

Compared to all others, the Vascular profile showed extensive subcortical atrophy and more cortical atrophy in regions such as the cingulate, lateral orbitofrontal, and postcentral areas (**Fig. 5A-B**). The Mixed profile had less cortical atrophy than all other profiles (β=0.50, p<.001) but exhibited more subcortical atrophy in the putamen and global pallidus. The NOVAS profile exhibited more severe atrophy at baseline compared to all other profiles (β=-1.21, p<.001). This atrophy was most pronounced in the frontal (middle and superior frontal), lateral temporal (inferior, middle, and superior temporal), and medial temporal (entorhinal cortex, hippocampus, and amygdala) regions. In line with this observation, CSF NfL levels were highest in the NOVAS profile (β=0.42, p<.001) and lowest in the αSyn profile (β=-0.28, p=0.004) compared to all other profiles (**Supplementary Figure 5**).

Functional connectivity

In terms of functional connectivity, the αSyn profile exhibited clearly lower global nodal strength compared to all other profiles (β=-0.45, p<.001) (**Fig. 5C**). Regional analyses revealed that this reduction in nodal strength was widespread across the cortex (**Fig. 5D**) and across all networks (**Supplementary Fig. 6**). No differences were observed for any of the other profiles.

White matter integrity

Global white matter integrity measured as MD, on the other hand, was reduced in Mixed (β=0.36, p<.001) and Vascular profiles compared to all other profiles (β=0.50, p<.001) (**Fig. 5E**). These

white matter changes were diffuse with an emphasis around the periventricular white matter (**Fig. 5F**). Additionally, the NOVAS profile showed lower white matter integrity in lateral temporal regions compared to all other profiles. Similar results were found for functional anisotropy (FA) (**Supplementary Fig. 7**).

Adjusting analyses for cognitive state at baseline yielded highly similar results (**Supplementary Fig. 8**).

Biomarker profiles are associated with different rates of clinical progression

The AD biomarker profile exhibited a faster decline in global cognition, as measured by the MMSE, compared to all other profiles (β=-0.08, p_{FDR}=.005) (**Fig. 4**). The αSyn profile declined faster in language (categorical fluency test) (β=-0.02, p_{FDR}=.018), executive functioning (TMT B-A) (β=0.07, p_{FDR}=.012), and visuospatial functioning (VOSP) (β=-0.12, p_{FDR}=.018). No other significant longitudinal differences were observed. Detailed longitudinal statistical comparisons are provided in **Supplementary Table 12**. Results from models adjusted for cognitive baseline status were largely consistent (**Supplementary Table 13**).

Discussion

In this study, we employed a data-driven approach to develop a biological framework that categorizes individuals from a heterogenous memory clinic cohort based on the presence, extent, and sequence of several common pathologies, using a multimodal biomarker array. The data-driven approach resulted in five major biomarker profiles, which we termed AD, Vascular, Mixed, αSyn, and NOVAS. These profiles captured disease progression patterns with clinico-pathological characteristics resembling prevalent neurodegenerative diseases (AD, αSyn, and Vascular profiles), as well as comorbid pathologies (Mixed profile), and a heterogenous group of individuals exhibiting atrophy without major pathologies detected by the available biomarkers (NOVAS profile). The different biomarker profiles are summarized in **Fig. 6**.

Our data-driven framework builds upon the recently updated AA criteria for the diagnosis and staging of AD[5] and the neuronal α-synuclein disease integrated staging system (NSD-ISS)[73], which define AD and neuronal α-synuclein-disease as biological processes that can be diagnosed solely via biomarkers. Using biomarkers that assess pathological changes as outlined in the AA criteria, we extended the framework to include other neurodegenerative diseases that occur within memory clinic cohorts. By integrating information on the extent and temporal sequence of pathologies, we classified individuals into distinct disease trajectories. This allowed us to differentiate individuals with similar biomarker statuses but differing primary etiologies. For instance, three distinct disease trajectories regarding AD and SVD emerged. Participants with early appearance of both pathologies exhibited lower levels of AD pathology and cortical atrophy compared to those with early AD pathology only, despite showing cognitive impairment. This could reflect additive or synergistic effects of multiple pathologies on cognitive function, leading to similar cognitive impairment despite a lower overall burden of AD pathology[74]. Alternatively, cognitive impairment in these individuals may be primarily driven by SVD, with a high WMH burden alongside subcortical atrophy and reduced white matter integrity playing an important role[75]. More work is needed to understand the effect of each pathology on clinical outcomes to inform the selection of participants, optimize trial design, and improve the evaluation of therapeutic efficiency.

Our findings align with prior research indicating that a biological definition of neurodegenerative diseases may improve diagnostic accuracy and prognostic precision. Within our memory clinic cohort, 14.3% of participants had an unclear or unknown clinical diagnosis. Applying our data-driven biological framework allowed us to classify these individuals according to their most likely disease progression trajectory. Notably, within the 14.3% of participants with an undetermined clinical diagnosis, the Vascular and NOVAS biomarker profiles accounted for the highest proportions (26.9% and 25.7%, respectively). The NOVAS profile comprised individuals with atrophy but no or minimal pathology using available biomarkers, suggesting that their clinical symptoms may be partly attributable to other neuropathologies not detected or quantified here. In line, a large proportion of the NOVAS profile had clinical diagnoses including frontotemporal dementia (FTD) and Progressive Supranuclear Palsy (PSP), which currently lack biomarkers of the underlying pathology. Another potential contributor is Limbic-predominant Age-related TDP-43 Encephalopathy (LATE). LATE usually affects older people (age>80 years) and is characterized by disproportionate limbic atrophy and memory impairments[76]. This aligns with the

older age, more pronounced hippocampal and amygdala atrophy, structural connectivity disruptions in temporal regions, and greater baseline memory deficits observed in the NOVAS profile. Emerging plasma biomarkers for TDP-43 have shown promising first results[77] and it will be of great interest to validate this study's findings when such a biomarker becomes available. Taken together, the identification of this group of neurodegenerative diseases that lack biomarkers further underscores the need for accurate biomarkers to improve disease classification.

The clinical usefulness of such biomarker-based profiles extends beyond diagnostic classification as they might offer insights into therapeutic stratification and clinical prognosis as well. Neurodegenerative diseases are often characterized by the presence of multiple neuropathologies, with approximately 80% of patients, especially older individuals, having one or more comorbid pathologies in the brain[19,22-26,78]. Consistently, we found that many participants in our cohort showed biomarker evidence of mixed pathologies, as individuals assigned to specific biomarker profiles often showed additional biomarker abnormalities indicative of other pathological processes. For instance, among individuals with an assigned αSyn biomarker profile, ~63% also showed abnormal Aβ, ~26% had abnormal tau, and ~30% had WMLs. The high prevalence of Aβ- and tau-positivity in this group is in line with previous studies reporting a high co-occurrence of AD and LBP, with up to 75% of patients with a Lewy body disease (LBD) showing AD co-pathology[79,80] and with up to 60% of AD patients showing LB co-pathology[81,82]. When co-occurring in the same individual, AD and LBP may interact with each other and promote each other's progression[83,84] due to the cross-seeding abilities of misfolded protein aggregates[85,86] or shared underlying pathological pathways[87,88]. The presence of concomitant pathologies are often not benign, as several previous studies have shown that the presence of multiple pathologies may have additive or even synergistic effects on cognitive decline[26,28,29]. This has important implications for individual prognosis, the selection of appropriate candidates for treatment, and interpretation of clinical trial results. For example, individuals with mixed pathology are more likely to show faster rates of disease progression and worse response to treatments targeting one specific pathology and might benefit more from combination therapies. Taken together, by integrating these multi-biomarker-based classifications into clinical decision-making, patient counseling could be refined, trial stratification could be improved, and the evaluation of therapeutic efficacy in the context of precision medicine could be enhanced.

Another disease group warranting further research is Lewy body disease, represented here by the αSyn profile. Historically, the lack of reliable *in vivo* biomarkers for Lewy body pathology has limited both cross-sectional and longitudinal studies in individuals with biomarker-confirmed primary or comorbid neuronal α-synuclein pathology. In this study, we thoroughly characterized individuals with neuronal α-synuclein pathology. Notably, we observed lower overall functional connectivity in the αSyn profile compared to all other profiles, despite having less cortical atrophy and better white matter integrity. This aligns with prior research indicating that patients with a Lewy body disease and cognitive impairment spend more time in hypoconnectivity states than normal controls[89-92]. Disturbances in brain connectivity have been attributed to deficits in the cholinergic and dopaminergic systems, resulting from nigral and basal forebrain degeneration[93]. These dopaminergic and cholinergic deficits have been linked to executive impairments seen in Lewy body diseases, which is consistent with the faster cognitive decline in executive functioning observed in the αSyn profile in the current study. Thus, disruptions in functional brain connectivity due to deficits in neurotransmitter systems may underly cognitive impairments associated with Lewy body disease.

This study has several limitations. First, the identified biomarker profiles are dependent on cohort composition and the biomarkers available. While the BioFINDER-2 cohort includes a broad range of clinical diagnoses and biomarkers, results may be influenced by recruitment bias and may vary in cohorts with differing characteristics. Second, the choice of cognitive tests may have influenced the observed cognitive differences, as different tests capture distinct aspects of cognitive impairment. Third, it is possible that variations in sensitivity of the included biomarkers might have influenced the inferred temporal sequence of biomarkers shifting from normal to pathological. Fourth, the SuStaIn method assumes that all biomarkers reach abnormality during the disease progression within each biomarker profile, which may not always hold true. Finally, while we accounted for the level of pathological burden for most biomarkers, this was not possible for CSF SAA, which detects only the presence or absence of α-synuclein.

In conclusion, we describe five data-driven biomarker-based profiles of neurodegeneration, combining information on biomarker status and disease progression. Our results suggest that the ordering of (co-)pathologies holds meaningful information besides the simple presence of these pathologies, making a distinction between the dominant or primary pathology and subsequent comorbidities that could explain individual variation in disease trajectories. Such a framework

could be useful in the clinical settings, where it could support patient selection for therapeutic intervention and their expected clinical efficacy.

Data availability

Anonymized data from BioFINDER will be shared on request from a qualified academic investigator for the sole purpose of replicating procedures and results presented in the article and as long as data transfer is in agreement with EU legislation on the general data protection regulation and decisions by the Swedish Ethical Review Authority and Region Skåne, which should be regulated in a material transfer agreement.

Acknowledgements

We would like to acknowledge all BioFINDER team members. We kindly thank all participants in the BioFINDER study and their family members. The thumbnail image for the online table of contents was created in BioRender. Mastenbroek, S. (2025) https://BioRender.com/1hitd4e.

Funding

This work was funded by Alzheimer Nederland (WE.15-2022-04), the European Research Council under the European Union's Horizon 2020 research and innovation programme (949570, PI: R.O.), the Swedish Research Council (2018-02052, 2022-00775), ERA PerMed (ERAPERMED2021-184), the Knut and Alice Wallenberg foundation (2017-0383), the MultiPark - A Strategic Research Area at Lund University, the Swedish Alzheimerfonden (AF-980907, AF-981132, AF-1011949), the Swedish Brain Foundation (FO2021-0293, FO2022-0204, FO2024-0284), the Swedish Parkinsonfonden (1412/22), Bundy Academy, the Cure Alzheimer's fund, the Konung Gustaf V:s och Drottning Victorias Frimurarestiftelse, Familjen Rönnströms Stiftelse, Greta och Johan Kocks stiftelse, WASP and DDLS Joint call for research projects (WASP/DDLS22-066), Skånes universitetssjukhus (2020-O000028), Region Skåne (2022-1259) and the Swedish federal government under the ALF agreement (2022-Projekt0080, 2022-Projekt0107). This research was

funded in whole, or in part by the Wellcome Trust [227341/Z/23/Z]. For the purpose of open access, the author has applied a CC BY public copyright licence to any Author Accepted Manuscript version arising from this submission. Open access funding provided by Lund University.

Competing interests

OH is an employee of Eli Lilly and Lund University, and he has previously acquired research support (for Lund University) from AVID Radiopharmaceuticals, Biogen, C2N Diagnostics, Eli Lilly, Eisai, Fujirebio, GE Healthcare, and Roche. In the past 2 years, he has received consultancy/speaker fees from Alzpath, BioArctic, Biogen, Bristol Meyer Squibb, Eisai, Eli Lilly, Fujirebio, Merck, Novartis, Novo Nordisk, Roche, Sanofi and Siemens. L.E.C. has received research support from GE Healthcare and Springer Healthcare (paid to institution). F.B. acts as a consultant for Biogen-Idec, IXICO, Merck-Serono, Novartis, Combinostics, and Roche. He has received grants, or grants are pending, from the Amyloid Imaging to Prevent Alzheimer's Disease (AMYPAD) initiative, the Biomedical Research Centre at University College London Hospitals, the Dutch MS Society, ECTRIMS–MAGNIMS, EU-H2020, the Dutch Research Council (NWO), the UK MS Society, and the National Institute for Health Research, University College London. He has received payments for the development of educational presentations from Ixico and his institution from Biogen-Idec and Merck. He is on the editorial board of Radiology, European Neuroradiology, Multiple Sclerosis Journal, and Neurology. Is on the board of directors of Queen Square Analytics. R.O. has received research support from Avid Radiopharmaceuticals, has given lectures in symposia sponsored by GE Healthcare and is an editorial board member of Alzheimer's Research & Therapy and the European Journal of Nuclear Medicine and Molecular Imaging. S.P. has acquired research support (for the institution) from ki elements/Alzheimer Drug Discoveries Foundation. In the past 2 years he has received consultancy/speaker fees from Bioartic, Biogen, Eisai, Eli Lilly, Novo Nordisk, and Roche. NMC has received consultancy/speaker fees from Biogen, Eli Lilly, Owkin and Merck. The remaining authors declare no competing interests.

Supplementary material

Supplementary material is available at *Brain* online.

References

1 McKhann, G. *et al.* Clinical diagnosis of Alzheimer's disease. *Neurology* **34**, 939-939 (1984). https://doi.org:doi:10.1212/WNL.34.7.939

2 Chui, H. C. *et al.* Clinical Criteria for the Diagnosis of Vascular Dementia: A Multicenter Study of Comparability and Interrater Reliability. *Archives of Neurology* **57**, 191-196 (2000). https://doi.org:10.1001/archneur.57.2.191

3 McKeith, I. G. *et al.* Diagnosis and management of dementia with Lewy bodies: third report of the DLB Consortium. *Neurology* **65**, 1863-1872 (2005). https://doi.org:10.1212/01.wnl.0000187889.17253.b1

4 Postuma, R. B. *et al.* MDS clinical diagnostic criteria for Parkinson's disease. *Mov Disord* **30**, 1591-1601 (2015). https://doi.org:10.1002/mds.26424

5 Jack Jr., C. R. *et al.* Revised criteria for diagnosis and staging of Alzheimer's disease: Alzheimer's Association Workgroup. *Alzheimer's & Dementia* **20**, 5143-5169 (2024). https://doi.org:https://doi.org/10.1002/alz.13859

6 Höglinger, G. U. *et al.* A biological classification of Parkinson's disease: the SynNeurGe research diagnostic criteria. *The Lancet Neurology* **23**, 191-204 (2024). https://doi.org:10.1016/S1474-4422(23)00404-0

7 Hansson, O. Biomarkers for neurodegenerative diseases. *Nature Medicine* **27**, 954-963 (2021). https://doi.org:10.1038/s41591-021-01382-x

8 Taylor, J. P. *et al.* New evidence on the management of Lewy body dementia. *Lancet Neurol* **19**, 157-169 (2020). https://doi.org:10.1016/s1474-4422(19)30153-x

9 DeTure, M. A. & Dickson, D. W. The neuropathological diagnosis of Alzheimer's disease. *Mol Neurodegener* **14**, 32 (2019). https://doi.org:10.1186/s13024-019-0333-5

10 Wardlaw, J. M. *et al.* Neuroimaging standards for research into small vessel disease and its contribution to ageing and neurodegeneration. *Lancet Neurol* **12**, 822-838 (2013). https://doi.org:10.1016/s1474-4422(13)70124-8

11 Duering, M. *et al.* Neuroimaging standards for research into small vessel disease—advances since 2013. *The Lancet Neurology* **22**, 602-618 (2023). https://doi.org:10.1016/S1474-4422(23)00131-X

12 Bellomo, G. *et al.* α-Synuclein Seed Amplification Assays for Diagnosing Synucleinopathies: The Way Forward. *Neurology* **99**, 195-205 (2022). https://doi.org:10.1212/wnl.0000000000200878

13 Bargar, C. *et al.* Streamlined alpha-synuclein RT-QuIC assay for various biospecimens in Parkinson's disease and dementia with Lewy bodies. *Acta Neuropathol Commun* **9**, 62 (2021). https://doi.org:10.1186/s40478-021-01175-w

14 Hall, S. *et al.* Performance of αSynuclein RT-QuIC in relation to neuropathological staging of Lewy body disease. *Acta Neuropathol Commun* **10**, 90 (2022). https://doi.org:10.1186/s40478-022-01388-7

15 Rossi, M. *et al.* Ultrasensitive RT-QuIC assay with high sensitivity and specificity for Lewy body-associated synucleinopathies. *Acta Neuropathol* **140**, 49-62 (2020). https://doi.org:10.1007/s00401-020-02160-8

16 Arnold, M. R. *et al.* α-Synuclein Seed Amplification in CSF and Brain from Patients with Different Brain Distributions of Pathological α-Synuclein in the Context of Co-Pathology and Non-LBD Diagnoses. *Ann Neurol* **92**, 650-662 (2022). https://doi.org:10.1002/ana.26453

17 Höglinger, G. U. *et al.* A biological classification of Parkinson's disease: the SynNeurGe research diagnostic criteria. *Lancet Neurol* **23**, 191-204 (2024). https://doi.org:10.1016/s1474-4422(23)00404-0

18 Jack, C. R., Jr. *et al.* NIA-AA Research Framework: Toward a biological definition of Alzheimer's disease. *Alzheimers Dement* **14**, 535-562 (2018). https://doi.org:10.1016/j.jalz.2018.02.018

19 Beach, T. G. & Malek-Ahmadi, M. Alzheimer's Disease Neuropathological Comorbidities are Common in the Younger-Old. *J Alzheimers Dis* **79**, 389-400 (2021). https://doi.org:10.3233/jad-201213

20 Coomans, E. M. *et al.* Interactions between vascular burden and amyloid-β pathology on trajectories of tau accumulation. *Brain* **147**, 949-960 (2024). https://doi.org:10.1093/brain/awad317

21 Hamilton, R. L. Lewy bodies in Alzheimer's disease: a neuropathological review of 145 cases using alpha-synuclein immunohistochemistry. *Brain Pathol* **10**, 378-384 (2000). https://doi.org:10.1111/j.1750-3639.2000.tb00269.x

22 Jellinger, K. A. & Attems, J. Prevalence of dementia disorders in the oldest-old: an autopsy study. *Acta Neuropathol* **119**, 421-433 (2010). https://doi.org:10.1007/s00401-010-0654-5

23 Robinson, J. L. *et al.* Pathological combinations in neurodegenerative disease are heterogeneous and disease-associated. *Brain* **146**, 2557-2569 (2023). https://doi.org:10.1093/brain/awad059

24 Schneider, J. A., Arvanitakis, Z., Bang, W. & Bennett, D. A. Mixed brain pathologies account for most dementia cases in community-dwelling older persons. *Neurology* **69**, 2197-2204 (2007). https://doi.org:10.1212/01.wnl.0000271090.28148.24

25 Robinson, J. L. *et al.* Neurodegenerative disease concomitant proteinopathies are prevalent, age-related and APOE4-associated. *Brain* **141**, 2181-2193 (2018). https://doi.org:10.1093/brain/awy146

26 Boyle, P. A. *et al.* Person-specific contribution of neuropathologies to cognitive loss in old age. *Ann Neurol* **83**, 74-83 (2018). https://doi.org:10.1002/ana.25123

27 Collij, L. E. *et al.* Lewy body pathology exacerbates brain hypometabolism and cognitive decline in Alzheimer's disease. *Nature Communications* **15**, 8061 (2024). https://doi.org:10.1038/s41467-024-52299-1

28 Palmqvist, S. *et al.* Cognitive effects of Lewy body pathology in clinically unimpaired individuals. *Nature Medicine* **29**, 1971-1978 (2023). https://doi.org:10.1038/s41591-023-02450-0

29 Quadalti, C. *et al.* Clinical effects of Lewy body pathology in cognitively impaired individuals. *Nat Med* **29**, 1964-1970 (2023). https://doi.org:10.1038/s41591-023-02449-7

30 Young, A. L. *et al.* Uncovering the heterogeneity and temporal complexity of neurodegenerative diseases with Subtype and Stage Inference. *Nature Communications* **9**, 4273 (2018). https://doi.org:10.1038/s41467-018-05892-0

31 Young, A. L. *et al.* Ordinal SuStaIn: Subtype and Stage Inference for Clinical Scores, Visual Ratings, and Other Ordinal Data. *Frontiers in Artificial Intelligence* **4** (2021). https://doi.org:10.3389/frai.2021.613261

32 Aksman, L. M. *et al.* pySuStaIn: a Python implementation of the Subtype and Stage Inference algorithm. *SoftwareX* **16** (2021). https://doi.org:10.1016/j.softx.2021.100811

33 Palmqvist, S. *et al.* Discriminative accuracy of plasma phospho-tau217 for Alzheimer disease vs other neurodegenerative disorders. *Jama* **324**, 772-781 (2020).

34 *Diagnostic and statistical manual of mental disorders : DSM-5™*. 5th edition. edn, (American Psychiatric Publishing, a division of American Psychiatric Association, 2013).

35 Borland, E., Stomrud, E., van Westen, D., Hansson, O. & Palmqvist, S. The age-related effect on cognitive performance in cognitively healthy elderly is mainly caused by underlying AD pathology or cerebrovascular lesions: implications for cutoffs regarding cognitive impairment. *Alzheimers Res Ther* **12**, 30 (2020). https://doi.org:10.1186/s13195-020-00592-8

36 Cummings, J. L., Dubois, B., Molinuevo, J. L. & Scheltens, P. International Work Group criteria for the diagnosis of Alzheimer disease. *Med Clin North Am* **97**, 363-368 (2013). https://doi.org:10.1016/j.mcna.2013.01.001

37 McKeith, I. G. *et al.* Diagnosis and management of dementia with Lewy bodies: Fourth consensus report of the DLB Consortium. *Neurology* **89**, 88-100 (2017). https://doi.org:10.1212/wnl.0000000000004058

38 McKeith, I. G. *et al.* Research criteria for the diagnosis of prodromal dementia with Lewy bodies. *Neurology* **94**, 743-755 (2020). https://doi.org:doi:10.1212/WNL.0000000000009323

39 Gelb, D. J., Oliver, E. & Gilman, S. Diagnostic criteria for Parkinson disease. *Arch Neurol* **56**, 33-39 (1999). https://doi.org:10.1001/archneur.56.1.33

40 Palmqvist, S. *et al.* Discriminative Accuracy of Plasma Phospho-tau217 for Alzheimer Disease vs Other Neurodegenerative Disorders. *Jama* **324**, 772-781 (2020). https://doi.org:10.1001/jama.2020.12134

41 Hansson, O. *et al.* CSF biomarkers of Alzheimer's disease concord with amyloid-β PET and predict clinical progression: A study of fully automated immunoassays in BioFINDER and ADNI cohorts. *Alzheimers Dement* **14**, 1470-1481 (2018). https://doi.org:10.1016/j.jalz.2018.01.010

42 Gobom, J. *et al.* Validation of the LUMIPULSE automated immunoassay for the measurement of core AD biomarkers in cerebrospinal fluid. *Clin Chem Lab Med* **60**, 207-219 (2022). https://doi.org:10.1515/cclm-2021-0651

43 Leuzy, A. *et al.* Diagnostic Performance of RO948 F 18 Tau Positron Emission Tomography in the Differentiation of Alzheimer Disease From Other Neurodegenerative Disorders. *JAMA Neurol* **77**, 955-965 (2020). https://doi.org:10.1001/jamaneurol.2020.0989

44 Cho, H. *et al.* In vivo cortical spreading pattern of tau and amyloid in the Alzheimer disease spectrum. *Ann Neurol* **80**, 247-258 (2016). https://doi.org:10.1002/ana.24711

45 Desikan, R. S. *et al.* An automated labeling system for subdividing the human cerebral cortex on MRI scans into gyral based regions of interest. *Neuroimage* **31**, 968-980 (2006). https://doi.org:10.1016/j.neuroimage.2006.01.021

46 Mattsson, N. *et al.* (18)F-AV-1451 and CSF T-tau and P-tau as biomarkers in Alzheimer's disease. *EMBO Mol Med* **9**, 1212-1223 (2017). https://doi.org:10.15252/emmm.201707809

47 Smith, S. M. *et al.* Advances in functional and structural MR image analysis and implementation as FSL. *Neuroimage* **23 Suppl 1**, S208-219 (2004). https://doi.org:10.1016/j.neuroimage.2004.07.051

48 Patenaude, B., Smith, S. M., Kennedy, D. N. & Jenkinson, M. A Bayesian model of shape and appearance for subcortical brain segmentation. *Neuroimage* **56**, 907-922 (2011). https://doi.org:10.1016/j.neuroimage.2011.02.046

49 Craddock, R. C. *et al.* Imaging human connectomes at the macroscale. *Nature Methods* **10**, 524-539 (2013). https://doi.org:10.1038/nmeth.2482

50 Berron, D. *et al.* Early stages of tau pathology and its associations with functional connectivity, atrophy and memory. *Brain* **144**, 2771-2783 (2021). https://doi.org:10.1093/brain/awab114

51 Friston, K. J., Williams, S., Howard, R., Frackowiak, R. S. & Turner, R. Movement-related effects in fMRI time-series. *Magn Reson Med* **35**, 346-355 (1996). https://doi.org:10.1002/mrm.1910350312

52 Behzadi, Y., Restom, K., Liau, J. & Liu, T. T. A component based noise correction method (CompCor) for BOLD and perfusion based fMRI. *Neuroimage* **37**, 90-101 (2007). https://doi.org:10.1016/j.neuroimage.2007.04.042

53 Power, J. D., Barnes, K. A., Snyder, A. Z., Schlaggar, B. L. & Petersen, S. E. Spurious but systematic correlations in functional connectivity MRI networks arise from subject motion. *Neuroimage* **59**, 2142-2154 (2012). https://doi.org:10.1016/j.neuroimage.2011.10.018

54 Schaefer, A. *et al.* Local-Global Parcellation of the Human Cerebral Cortex from Intrinsic Functional Connectivity MRI. *Cereb Cortex* **28**, 3095-3114 (2018). https://doi.org:10.1093/cercor/bhx179

55 Cole, M. W., Pathak, S. & Schneider, W. Identifying the brain's most globally connected regions. *NeuroImage* **49**, 3132-3148 (2010). https://doi.org:https://doi.org/10.1016/j.neuroimage.2009.11.001

56 Tournier, J. D. *et al.* MRtrix3: A fast, flexible and open software framework for medical image processing and visualisation. *Neuroimage* **202**, 116137 (2019). https://doi.org:10.1016/j.neuroimage.2019.116137

57 Basser, P. J., Mattiello, J. & Lebihan, D. Estimation of the Effective Self-Diffusion Tensor from the NMR Spin Echo. *Journal of Magnetic Resonance, Series B* **103**, 247-254 (1994). https://doi.org:https://doi.org/10.1006/jmrb.1994.1037

58 Basser, P. J., Mattiello, J. & LeBihan, D. MR diffusion tensor spectroscopy and imaging. *Biophys J* **66**, 259-267 (1994). https://doi.org:10.1016/s0006-3495(94)80775-1

59 Cerri, S. *et al.* A contrast-adaptive method for simultaneous whole-brain and lesion segmentation in multiple sclerosis. *Neuroimage* **225**, 117471 (2021). https://doi.org:10.1016/j.neuroimage.2020.117471

60 Hristovska, I. *et al.* Identification of distinct and shared biomarker panels in different manifestations of cerebral small vessel disease through proteomic profiling. *medRxiv* (2024). https://doi.org:10.1101/2024.06.10.24308599

61 Sudre, C. H. *et al.* Bayesian model selection for pathological neuroimaging data applied to white matter lesion segmentation. *IEEE Trans Med Imaging* **34**, 2079-2102 (2015). https://doi.org:10.1109/tmi.2015.2419072

62 D'Agostino, R. B., Sr. *et al.* General cardiovascular risk profile for use in primary care: the Framingham Heart Study. *Circulation* **117**, 743-753 (2008). https://doi.org:10.1161/circulationaha.107.699579

63 Cantone, E., Maione, N., Di Rubbo, V., Esposito, F. & Iengo, M. Olfactory performance after crenotherapy in chronic rhinosinusitis in the elderly. *Laryngoscope* **125**, 1529-1534 (2015). https://doi.org:10.1002/lary.25173

64 Åstrand, R., Rolstad, S. & Wallin, A. Cognitive Impairment Questionnaire (CIMP-QUEST): reported topographic symptoms in MCI and dementia. *Acta Neurologica Scandinavica* **121**, 384-391 (2010). https://doi.org:https://doi.org/10.1111/j.1600-0404.2009.01312.x

65 Ismail, Z. *et al.* The Mild Behavioral Impairment Checklist (MBI-C): A Rating Scale for Neuropsychiatric Symptoms in Pre-Dementia Populations. *J Alzheimers Dis* **56**, 929-938 (2017). https://doi.org:10.3233/jad-160979

66 Zigmond, A. S. & Snaith, R. P. The hospital anxiety and depression scale. *Acta Psychiatr Scand* **67**, 361-370 (1983). https://doi.org:10.1111/j.1600-0447.1983.tb09716.x

67 Mastenbroek, S. E. *et al.* Disease progression modelling reveals heterogeneity in trajectories of Lewy-type α-synuclein pathology. *bioRxiv*, 2023.2012.2005.569878 (2023). https://doi.org:10.1101/2023.12.05.569878

68 Young, A. L. *et al.* Data-driven neuropathological staging and subtyping of TDP-43 proteinopathies. *Brain* (2023). https://doi.org:10.1093/brain/awad145

69 Collij, L. E. *et al.* Spatial-Temporal Patterns of β-Amyloid Accumulation: A Subtype and Stage Inference Model Analysis. *Neurology* **98**, e1692-e1703 (2022). https://doi.org:10.1212/wnl.0000000000200148

70 Vogel, J. W. *et al.* Four distinct trajectories of tau deposition identified in Alzheimer's disease. *Nature Medicine* **27**, 871-881 (2021). https://doi.org:10.1038/s41591-021-01309-6

71 Smith, S. M. *et al.* Tract-based spatial statistics: voxelwise analysis of multi-subject diffusion data. *Neuroimage* **31**, 1487-1505 (2006). https://doi.org:10.1016/j.neuroimage.2006.02.024

72 RStudio, T. RStudio: integrated development for R. *RStudio, Inc., Boston, MA URL http//www.rstudio.com* **42**, 84 (2015).

73 Simuni, T. *et al.* A biological definition of neuronal α-synuclein disease: towards an integrated staging system for research. *The Lancet Neurology* **23**, 178-190 (2024). https://doi.org:https://doi.org/10.1016/S1474-4422(23)00405-2

74 Landau, S. M. *et al.* Individuals with Alzheimer's disease and low tau burden: Characteristics and implications. *Alzheimer's & Dementia* **20**, 2113-2127 (2024). https://doi.org:https://doi.org/10.1002/alz.13609

75 Hamilton, O. K. L. *et al.* Cognitive impairment in sporadic cerebral small vessel disease: A systematic review and meta-analysis. *Alzheimers Dement* **17**, 665-685 (2021). https://doi.org:10.1002/alz.12221

76 Nelson, P. T. *et al.* Limbic-predominant age-related TDP-43 encephalopathy (LATE): consensus working group report. *Brain* **142**, 1503-1527 (2019). https://doi.org:10.1093/brain/awz099

77 Chatterjee, M. *et al.* Plasma extracellular vesicle tau and TDP-43 as diagnostic biomarkers in FTD and ALS. *Nature Medicine* **30**, 1771-1783 (2024). https://doi.org:10.1038/s41591-024-02937-4

78 Karanth, S. *et al.* Prevalence and Clinical Phenotype of Quadruple Misfolded Proteins in Older Adults. *JAMA Neurol* **77**, 1299-1307 (2020). https://doi.org:10.1001/jamaneurol.2020.1741

79 Graff-Radford, J. *et al.* Duration and Pathologic Correlates of Lewy Body Disease. *JAMA Neurol* **74**, 310-315 (2017). https://doi.org:10.1001/jamaneurol.2016.4926

80 Sabbagh, M. N. *et al.* Parkinson disease with dementia: comparing patients with and without Alzheimer pathology. *Alzheimer Dis Assoc Disord* **23**, 295-297 (2009). https://doi.org:10.1097/WAD.0b013e31819c5ef4

81 Savica, R. *et al.* Lewy body pathology in Alzheimer's disease: A clinicopathological prospective study. *Acta Neurol Scand* **139**, 76-81 (2019). https://doi.org:10.1111/ane.13028

82 Kotzbauer, P. T., Trojanowsk, J. Q. & Lee, V. M. Lewy body pathology in Alzheimer's disease. *J Mol Neurosci* **17**, 225-232 (2001). https://doi.org:10.1385/jmn:17:2:225

83 van der Gaag, B. L. *et al.* Distinct tau and alpha-synuclein molecular signatures in Alzheimer's disease with and without Lewy bodies and Parkinson's disease with dementia. *Acta Neuropathologica* **147**, 14 (2024). https://doi.org:10.1007/s00401-023-02657-y

84 Lashley, T. *et al.* Cortical alpha-synuclein load is associated with amyloid-beta plaque burden in a subset of Parkinson's disease patients. *Acta Neuropathol* **115**, 417-425 (2008). https://doi.org:10.1007/s00401-007-0336-0

85 Masliah, E., Iwai, A., Mallory, M., Uéda, K. & Saitoh, T. Altered presynaptic protein NACP is associated with plaque formation and neurodegeneration in Alzheimer's disease. *Am J Pathol* **148**, 201-210 (1996).

86 Guo, J. L. *et al.* Distinct α-synuclein strains differentially promote tau inclusions in neurons. *Cell* **154**, 103-117 (2013). https://doi.org:10.1016/j.cell.2013.05.057

87 Bellomo, G., Paciotti, S., Gatticchi, L. & Parnetti, L. The vicious cycle between α-synuclein aggregation and autophagic-lysosomal dysfunction. *Mov Disord* **35**, 34-44 (2020). https://doi.org:10.1002/mds.27895

88 Van Acker, Z. P., Bretou, M. & Annaert, W. Endo-lysosomal dysregulations and late-onset Alzheimer's disease: impact of genetic risk factors. *Mol Neurodegener* **14**, 20 (2019). https://doi.org:10.1186/s13024-019-0323-7

89 Schumacher, J. *et al.* Functional connectivity in mild cognitive impairment with Lewy bodies. *J Neurol* **268**, 4707-4720 (2021). https://doi.org:10.1007/s00415-021-10580-z

90 Díez-Cirarda, M. *et al.* Dynamic functional connectivity in Parkinson's disease patients with mild cognitive impairment and normal cognition. *Neuroimage Clin* **17**, 847-855 (2018). https://doi.org:10.1016/j.nicl.2017.12.013

91 Schumacher, J. *et al.* Dynamic functional connectivity changes in dementia with Lewy bodies and Alzheimer's disease. *Neuroimage Clin* **22**, 101812 (2019). https://doi.org:10.1016/j.nicl.2019.101812

92 Schumacher, J. *et al.* Dysfunctional brain dynamics and their origin in Lewy body dementia. *Brain* **142**, 1767-1782 (2019). https://doi.org:10.1093/brain/awz069

93 Bohnen, N. I. & Albin, R. L. The cholinergic system and Parkinson disease. *Behav Brain Res* **221**, 564-573 (2011). https://doi.org:10.1016/j.bbr.2009.12.048

Figure legends

Figure 1 Flow chart of participant selection from the complete BioFINDER-2 memory clinic cohort. Aβ = amyloid-β; CSF = cerebrospinal fluid; CU = cognitively unimpaired; MCI = mild cognitive impairment; MRI = magnetic resonance imaging; PET = positron emission tomography; SAA = seed amplification assay; SCD = subjective cognitive decline; SuStaIn = subtype and stage inference model.

Figure 2 Five biomarker profiles based on the temporal evolution of Aβ, tau, neuronal α-Synuclein, and WMHs. Five distinct biomarker profiles were identified and termed "AD", "α-Synuclein (αSyn), "Vascular", "Mixed AD & Vascular (Mixed)", and "Non-Vascular-Alzheimer-Synuclein (NOVAS)". Cross-validated positional variance diagrams are shown. Each box represents the certainty that a biomarker has reached abnormality at a given SuStaIn stage, with a higher opacity reflecting more confidence. Red indicates abnormal biomarker levels regarding CSF Aβ42/Aβ40 and CSF α-Syn, and abnormal low for all others. Magenta indicates abnormal high levels. Sample sizes are based on cognitive impaired individuals only (SCD, MCI, or dementia). Aβ = amyloid-β; AD = Alzheimer's disease; αSyn = α-Synuclein; CSF = cerebrospinal fluid; CT = cortical thickness; PET = positron emission tomography; SuStaIn = subtype and stage inference model; vol = volume; WMH = white matter hyperintensities.

Figure 3 Clinical diagnosis across biomarker profiles. Stacked barplots represent biomarker profile differences in the percentage of subjects with a clinical diagnosis specified by the color legend. Undetermined includes both individuals with MCI and dementia. Numbers represent the number of subjects (%).

Figure 4 Baseline cognitive performance and longitudinal clinical progression differs across biomarker profiles. Biomarker profile comparisons on baseline and longitudinal cognition. Lines represent model fits from linear mixed models corrected for baseline age, sex, and level of education. Sample sizes per test are shown in **Supplementary Table 1**. The clinical summary shows an overview of clinical domains affected at baseline and longitudinally in each biomarker profile as compared to all others. The healthy aging reference group consisted of cognitively unimpaired individuals without biomarker abnormalities and age>60 years and is displayed for visualization purposes only. *p_{FDR}<0.05, **p_{FDR}<0.01, ***p_{FDR}<0.001 vs. all others. CIMP-QUEST = Cognitive Impairment Questionnaire; HADS = Hospital Anxiety and Depression Scale; MMSE = Mini-Mental State Examination; SDMT = symbol digit modalities test; TMT = trail making test: VOSP = Visual Object and Space Perception.

Figure 5 Distinct atrophy, white matter integrity, and functional connectivity patterns in different biomarker profiles. Baseline comparisons on (**A**) global cortical thickness (*n*=787) measured in mm; (**B**) regional cortical thickness (*n*=787) and subcortical volumes (*n*=672); (**C**) global nodal strength (*n*=581) measured as the average Pearson correlation coefficient; (**D**) regional nodal strength (*n*=581); (**E**) global mean diffusivity (MD) (*n*=711) measured as the average mean diffusivity x10^{-3} mm^2/s; and (**F**) regional MD (*n*=711). All comparisons were corrected for baseline age and sex. In panels B, D, and F only regions that survived FDR-correction are shown. In B and D grey indicates non-significant regions. In F grey shows non-significant tracts. The healthy aging reference group consisted of cognitively unimpaired individuals without biomarker abnormalities and age>60 years and is displayed for visualization purposes only. *p<0.05, **p<0.01, ***p <0.001 vs. all others.

Figure 6 Summary of data-driven biomarker profiles identified in the BioFINDER-2 cohort.

A summary figure of the main characteristics associated with the five identified biomarker profiles. Aβ = amyloid-β; AD = Alzheimer's disease; NOVAS = Non-Vascular-Alzheimer-Synuclein.

Table 1 Sample characteristics

	Reference (*n*=143)	AD (n=317)	αSyn (n=123)	Vascular (n=67)	Mixed (n=207)	NOVAS (*n*=74)
Demographics						
Cognitive status, n (%)						
CU	143 (100%)	0 (0%)	0 (0%)	0 (0%)	0 (0%)	0 (0%)
SCD	0 (0%)	68 (21.5%)	20 (16.3%)	8 (11.9%)	51 (24.6%)*	5 (6.8%)*
MCI	0 (0%)	105 (33.1%)*	50 (40.7%)	33 (49.3%)	83 (40.1%)	27 (36.5%)
Dementia	0 (0%)	144 (45.4%)	53 (43.1%)	26 (38.8%)	73 (35.3%)*	42 (56.8%)*
Age, years	72.3 [12.3]	71.4 [11.8]*	73.1 [8.05]*	74.9 [6.12]*	75.2 [6.98]*	76.5 [7.59]*
Sex, n (%) female	82 (57.3%)	173 (54.6%)*	36 (29.3%)*	16 (23.9%)*	95 (45.9%)	32 (43.2%)
Education, years	12.0 [3.00]	12.0 [7.00]	14.0 [6.00]*	12.0 [5.75]	12.0 [6.00]	12.0 [7.00]
MMSE, baseline score	29.0 [1.00]	26.0 [8.00]*	27.0 [5.00]	26.0 [4.50]	27.0 [5.00]*	25.0 [5.75]*
APOE ε4 carrier, n (%)	44 (39.3%)	229 (72.9%)*	58 (47.9%)	22 (32.8%)*	98 (47.6%)*	30 (40.5%)*
APOE ε2 carrier, n (%)	15 (13.4%)	16 (5.1%)*	11 (9.1%)	8 (11.9%)	28 (13.6%)*	4 (5.4%)
FHS-CVD risk, %	25.8 [20.5]	29.0 [25.4]*	34.0 [25.8]	50.3 [28.3]*	37.1 [24.7]*	37.5 [23.0]
Diabetes, n (%)	8 (5.7%)	40 (13.6%)	12 (10.4%)	16 (24.2%)*	27 (13.9%)	16 (23.5%)
Hypertension, n (%)	62 (44.6%)	134 (45.4%)*	52 (44.8%)	39 (59.1%)	111 (57.2%)*	35 (51.5%)
Biomarker abnormality						
CSF $A\beta_{42}/A\beta_{40}$, n (%)	0 (100%)	316 (99.7%)*	77 (62.6%)*	20 (29.9%)*	114 (55.1%)*	51 (68.9%)
Tau-PET, n (%)						
Normal	143 (100%)	102 (32.2%)*	91 (74.0%)*	63 (94.0%)*	135 (65.2%)*	70 (94.6%)*
Positive low group	0 (0%)	74 (23.3%)*	27 (22.0%)	4 (6.0%)*	35 (16.9%)	4 (5.4%)*
Positive high group	0 (0%)	141 (44.5%)*	5 (4.1%)*	0 (0%)*	37 (17.9%)*	0 (0%)*
AD signature CT, n (%)						
Normal	143 (100%)	207 (65.3%)	98 (79.7%)*	50 (74.6%)	162 (78.3%)*	0 (0%)*
Positive low group	0 (0%)	41 (12.9%)	16 (13.0%)	12 (17.9%)	31 (15.0%)	24 (32.4%)*
Positive high group	0 (0%)	69 (21.8%)	9 (7.3%)*	5 (7.5%)*	14 (6.8%)*	50 (67.6%)*
Global CT, n (%)						
Normal	143 (100%)	253 (79.8%)	95 (77.2%)	47 (70.1%)	198 (95.7%)*	11 (14.9%)*
Positive low group	0 (0%)	22 (6.9%)	18 (14.6%)	10 (14.9%)	7 (3.4%)	24 (32.4%)
Positive high group	0 (0%)	42 (13.2%)	10 (8.1%)	10 (14.9%)	2 (1.0%)	39 (52.7%)
Lateral ventricular, n (%)						
Normal	143 (100%)	297 (93.7%)*	95 (77.2%)	0 (0%)*	171 (82.6%)	70 (94.6%)*
Positive low group	0 (0%)	20 (6.3%)	13 (10.6%)	10 (14.9%)	23 (11.1%)	4 (5.4%)
Positive high group	0 (0%)	0 (0%)*	15 (12.2%)	57 (85.1%)*	13 (6.3%)*	0 (0%)*
WMH volume, n (%)						
Normal	143 (100%)	269 (84.9%)*	86 (69.9%)*	9 (13.4%)*	0 (0%)*	51 (55.4%)
Positive low group	0 (0%)	35 (11.0%)*	35 (28.5%)*	25 (37.3%)*	48 (23.2%)	15 (20.3%)
Positive high group	0 (0%)	13 (4.1%)*	2 (1.6%)*	33 (49.3%)*	159 (76.8%)*	18 (24.3%)
CSF αSyn SAA, n (%)	0 (0%)	29 (9.1%)*	109 (88.6%)*	13 (19.4%)	35 (16.9%)*	16 (21.6%)

Data are presented as median [IQR] unless otherwise specified. Biomarker-positive groups were divided into low and high burden groups by a median split for tau, vascular, and atrophy biomarkers. The healthy aging reference group (denoted as reference) consisted of cognitively

unimpaired individuals without biomarker abnormalities and age>60 years. Biomarker profile groups (excluding the healthy reference group) were compared based on Kruskal-Wallis and chi-squared tests for continuous and categorical variables. Aβ = amyloid-β; αSyn = α-Synuclein; AD = Alzheimer's disease; CT = cortical thickness; CU = cognitively unimpaired; MCI = mild cognitive impairment; Mixed = Mixed AD & Vascular; MMSE = mini-mental state examination; NOVAS = non-Vascular-Alzheimer-Synuclein; PET = positron emission tomography; SAA = seeding amplification assay; WMH = white matter hyperintensities.
*p<0.05 versus all others.

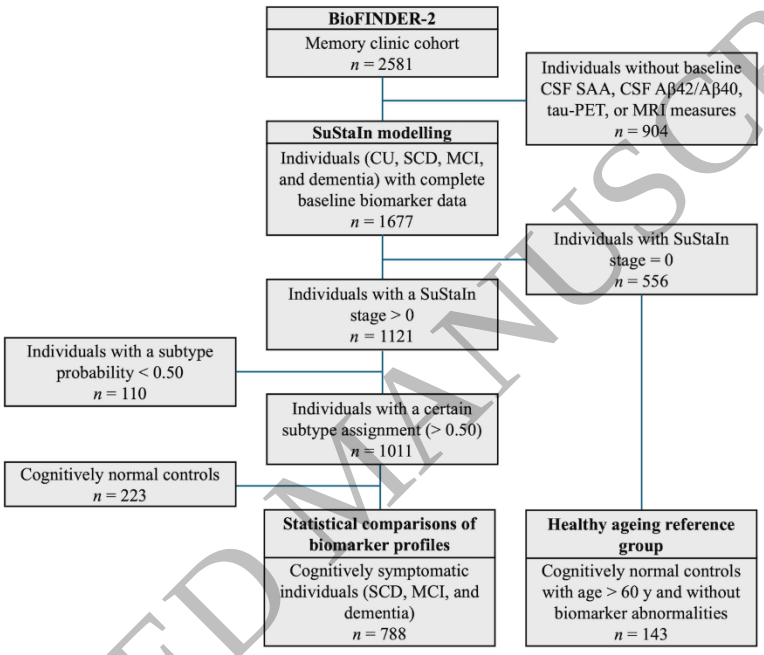

Figure 1
100x87 mm (x DPI)

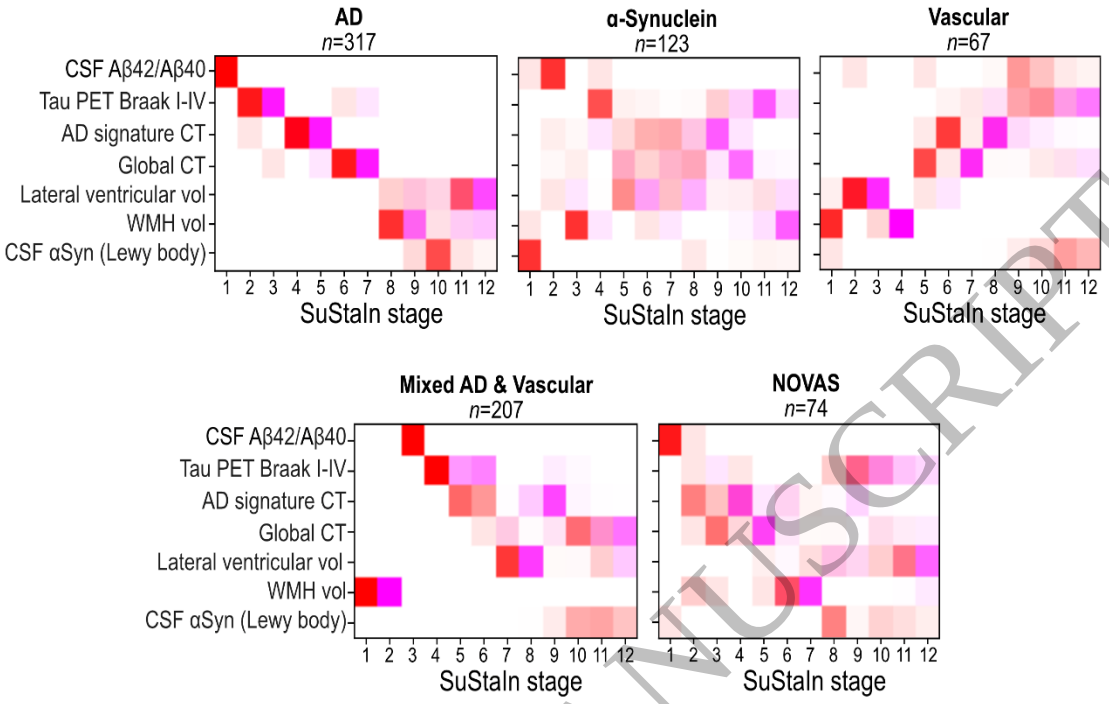

Figure 2
242x126 mm (x DPI)

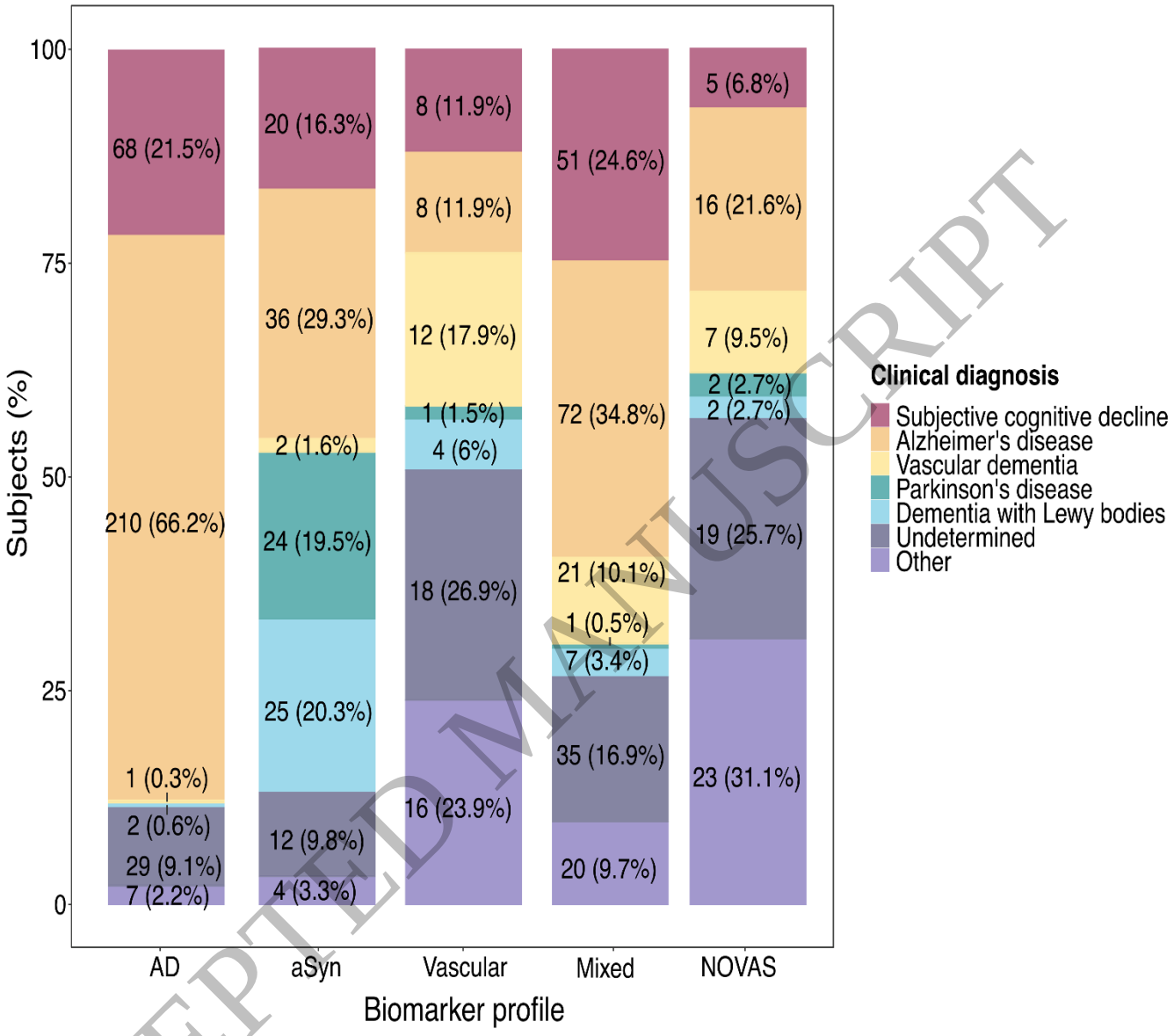

Figure 3
377x265 mm (x DPI)

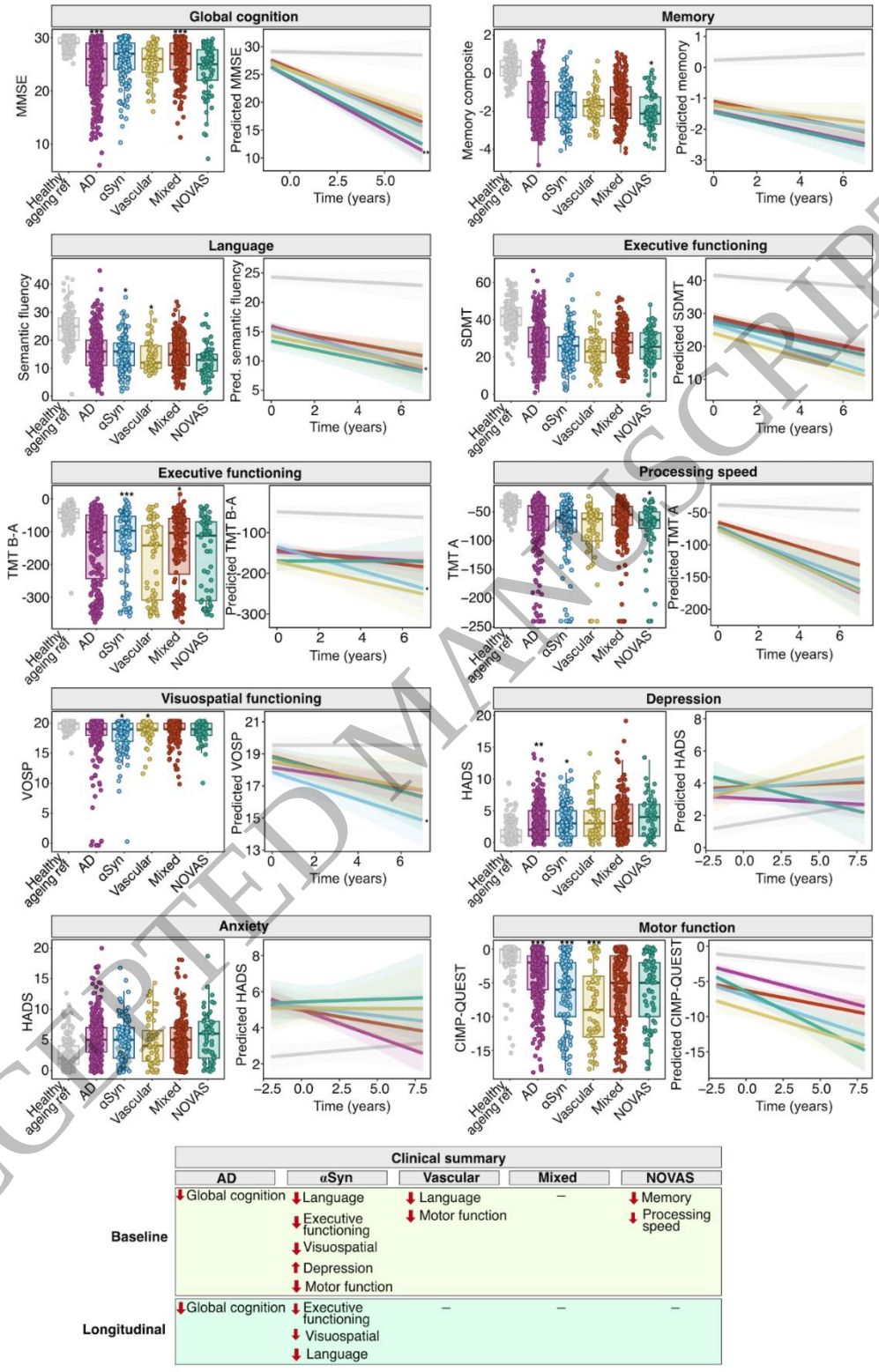

Figure 4
162x240 mm (x DPI)

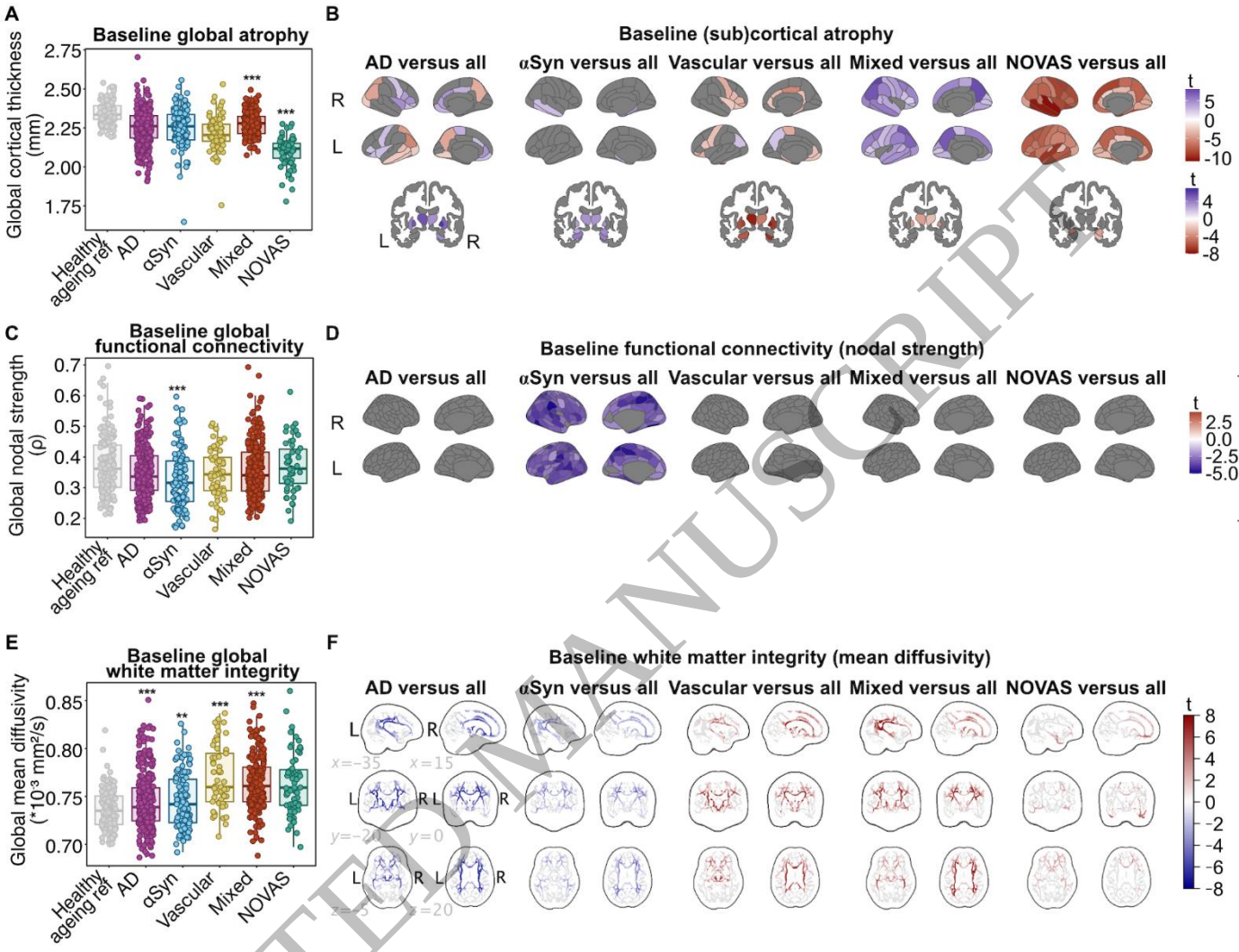

Figure 5
185x142 mm (x DPI)

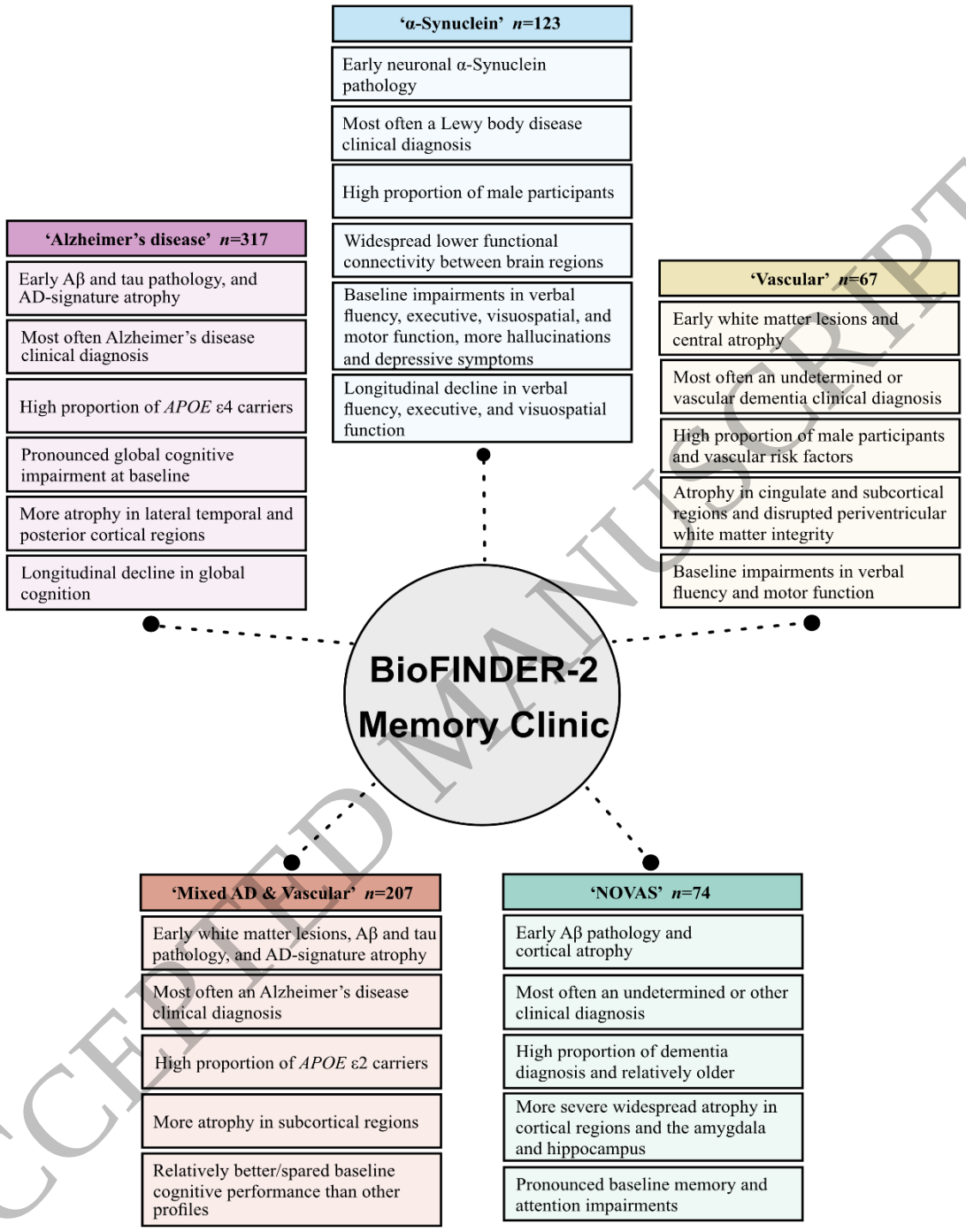

Figure 6
224x293 mm (x DPI)